

This article was downloaded by: [Universität Stuttgart]

On: 27 April 2015, At: 23:53

Publisher: Taylor & Francis

Informa Ltd Registered in England and Wales Registered Number: 1072954 Registered office: Mortimer House, 37-41 Mortimer Street, London W1T 3JH, UK



## Quantitative InfraRed Thermography Journal

Publication details, including instructions for authors and subscription information:

<http://www.tandfonline.com/loi/tqrt20>

### Highly-efficient and noncontact vibro-thermography via local defect resonance

Igor Solodov<sup>a</sup>, Markus Rahammer<sup>a</sup>, Daria Derusova<sup>b</sup> & Gerd Busse<sup>a</sup>

<sup>a</sup> Institute of Polymer Technology, Non-Destructive Testing (IKT), University of Stuttgart, Stuttgart, Germany

<sup>b</sup> National Research Tomsk Polytechnic University, Tomsk, Russian Federation

Published online: 27 Apr 2015.



[Click for updates](#)

To cite this article: Igor Solodov, Markus Rahammer, Daria Derusova & Gerd Busse (2015): Highly-efficient and noncontact vibro-thermography via local defect resonance, Quantitative InfraRed Thermography Journal, DOI: [10.1080/17686733.2015.1026018](https://doi.org/10.1080/17686733.2015.1026018)

To link to this article: <http://dx.doi.org/10.1080/17686733.2015.1026018>

PLEASE SCROLL DOWN FOR ARTICLE

Taylor & Francis makes every effort to ensure the accuracy of all the information (the "Content") contained in the publications on our platform. However, Taylor & Francis, our agents, and our licensors make no representations or warranties whatsoever as to the accuracy, completeness, or suitability for any purpose of the Content. Any opinions and views expressed in this publication are the opinions and views of the authors, and are not the views of or endorsed by Taylor & Francis. The accuracy of the Content should not be relied upon and should be independently verified with primary sources of information. Taylor and Francis shall not be liable for any losses, actions, claims, proceedings, demands, costs, expenses, damages, and other liabilities whatsoever or howsoever caused arising directly or indirectly in connection with, in relation to or arising out of the use of the Content.

This article may be used for research, teaching, and private study purposes. Any substantial or systematic reproduction, redistribution, reselling, loan, sub-licensing, systematic supply, or distribution in any form to anyone is expressly forbidden. Terms &



## Highly-efficient and noncontact vibro-thermography via local defect resonance

Igor Solodov<sup>a</sup>, Markus Rahammer<sup>a\*</sup>, Daria Derusova<sup>b</sup> and Gerd Busse<sup>a</sup>

<sup>a</sup>*Institute of Polymer Technology, Non-Destructive Testing (IKT), University of Stuttgart, Stuttgart, Germany;* <sup>b</sup>*National Research Tomsk Polytechnic University, Tomsk, Russian Federation*

(Received 27 October 2014; accepted 17 February 2015)

A frequency match between the driving ultrasonic wave and characteristic frequency of a defect provides an efficient energy pumping from the wave directly into the defect (local defect resonance (LDR)). Due to a strong resonance amplification of the local vibrations, the LDR-driven defects exhibit a high-Q thermal response and enable to implement frequency-selective thermosonic imaging with an opportunity to distinguish between different defects by changing the driving frequency. The LDR-thermosonics requires much lower acoustic power to activate defects that makes it possible to avoid high-power ultrasonic instrumentation and even proceed to a remote ultrasonic thermography by using air-coupled ultrasonic excitation.

**Keywords:** infrared thermography; non-destructive evaluation; vibrothermography; local defect resonance

### 1. Introduction

Ultrasonic based methodologies are among the leaders in the number and areas of NDT applications, not least because of simple and reliable ultrasound generation techniques as well as relatively inexpensive low-power electronics involved. On the contrary, ultrasonic thermography (vibrothermography, thermosonics) stands apart from other ultrasonic NDT counterparts for their specific instrumentation. To provide a measurable temperature response, thermosonics traditionally relies on high-power ultrasonic equipment, which was originally designed for the purpose of plastic welding and includes kW-power supply (at fixed frequencies 20 or 40 kHz) and piezo-stack converters combined with ultrasonic boosters and horns.[1] The test specimen is usually pressed against the horn that results in unstable ultrasonic response and highly non-reproducible measurements. The reason for this ‘specificity’ is concerned with a low efficiency of ultrasound-heat conversion that is usually taken for granted without an effort to be optimized.

To make ultrasonic thermography compatible with conventional ultrasonic equipment would be a step on the way to extend its applicability in nondestructive inspection. To this end, an obvious task is to find out a feasibility of ultrasonic thermography in mW-acoustic power range typical for commercial ultrasonic applications.

In this paper, the solution is proposed by optimizing the ultrasonic excitation of defects via the concept of local defect resonance (LDR).[2] The LDR provides a selective

---

\*Corresponding author. Email: [markus.rahammer@ikt.uni-stuttgart.de](mailto:markus.rahammer@ikt.uni-stuttgart.de)

excitation of a defect area and results in an efficient energy pumping from the wave directly into the defect strongly increasing its vibration amplitude. To evaluate the efficiency of heat generation by the LDR vibration pattern, the damping model is then applied to thermosonics of simulated defects (flat-bottomed holes (FBH)). Both the calculations and experimental results confirm that thermal output within 1 K is feasible for inputs in the range of a few acoustic mW. By combining LDR with lock-in approach reliable thermosonic imaging is expected to advance in sub-mW range of inputs. This opens an opportunity for noncontact thermosonic imaging to be implemented by using air-coupled ultrasound.

## 2. LDR concept

The concept of LDR is based on the fact that inclusion of a defect leads to a local decrease in stiffness for a certain mass of the material in this area, which should manifest in a particular characteristic frequency of the defect. The LDR fundamental frequency can be introduced as a natural frequency of the defect with an effective rigidity  $K_{eff}$  and mass  $M_{eff}$ :  $f_0 = \frac{1}{2\pi} \sqrt{K_{eff} / M_{eff}}$ . To derive the expressions for  $K_{eff}$  and  $M_{eff}$  one could evaluate potential and kinetic vibration energy of the defect. This approach applied to a circular FBH (radius  $R$ , thickness  $h$ ) yields [3]:

$$K_{eff} = 192\pi D / R^2; \quad M_{eff} = 1.8m, \quad (1)$$

where  $D = Eh^3 / 12(1 - \nu^2)$  is the bending stiffness and  $m$  is the mass of the plate in the bottom of the defect.

Equation (1) are then combined to yield the LDR frequency for the circular FBH:

$$f_0 \approx \frac{1.6h}{R^2} \sqrt{\frac{E}{12\rho(1 - \nu^2)}}. \quad (2)$$

The phenomenology presented is a simplified approach, which nonetheless enables to clarify the physical nature of the LDR. The expression for  $f_0$  obtained above is applicable to evaluation of the fundamental resonance frequencies of the defects, like FBH as well as laminar defects in rolled sheet metals and delaminations in composites.

The problem in practical use of the analytical approach is concerned with the boundary conditions for the defect edges, which were assumed to be clamped in deriving Equation (2). This is apparently justifiable for ‘deep’ defects in plates, however, in a general case the analytical formulation presented above becomes problematic. Instead, a finite element (FEM) simulation was used to visualize the LDR vibration patterns and to evaluate the LDR frequencies.

The software COMSOL MULTIPHYSICS (physics package ‘structural dynamics,’ ‘eigenfrequency analysis’) was found to be suitable for analyzing the vibration characteristics of structures with defects and to determine the LDR frequencies. By using eigenfrequency analysis of the model, each possible resonance of vibrations in the plate can be found and the vibration patterns plotted. Figure 1(a) illustrates the vibration pattern at one of the specimen eigenfrequencies of 1.5 kHz. For a higher resonance frequency 10.4 kHz, a fundamental local resonance of a circular FBH is readily recognized (Figure 1(b)), followed by the higher-order LDR at the higher driving frequency of 23.25 kHz (Figure 1(c)).

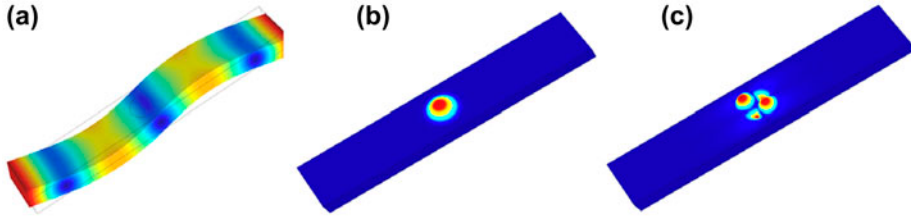


Figure 1. FEM simulations of vibration patterns of a PMMA plate (thickness 3 mm) with a FBH (radius 1 cm, depth 2 mm): 1.5 kHz plate eigenfrequency (a), fundamental LDR (10.4 kHz) (b), and higher-order LDR (23.25 kHz) (c).

### 3. Experimental evidence for LDR

A direct way to experimentally reveal LDR is to measure an individual contribution of each point of the specimen in its overall frequency response in a wide frequency range. For this purpose, an ultrasonic excitation by a wide-band piezoelectric transducer is combined with a laser vibrometer scan of the specimen surface. It enables to probe and indicate all possible resonances in the vibration spectrum of every point of the specimen. The origin of each maximum is then verified by imaging the vibration pattern at the corresponding frequency.

Figure 2 shows an example of the LDR frequency response (a) and the vibration pattern (b) measured for a FBH in a PMMA plate. A strong enhancement (about 20 dB) of the vibration amplitude with a high Q-factor ( $Q \approx 70$ ) observed locally in the defect area is identified as a fundamental defect resonance (Figure 2(a) and (b)). Such a methodology was successfully applied to a search for LDR in a variety of materials.[3] The two other examples presented in Figure 2(c) and (d) illustrate a clear evidence of LDR excited by propagating flexural waves in high kHz-frequency range for a simulated delamination (LDR frequency 91160 Hz) and an impact damage (LDR  $\sim 110000$  Hz) in carbon fiber reinforced plastic (CFRP). Similar LDR with local resonance ‘amplification’ of the vibration amplitude as high as  $\sim (20\text{--}40\text{ dB})$  were generally measured for other types of realistic defects.

### 4. Heat generation by LDR vibrations

In ultrasonic thermography, the defect thermal response is caused by a local dissipation of mechanical energy, which is converted into heat. For viscoelastic materials, this

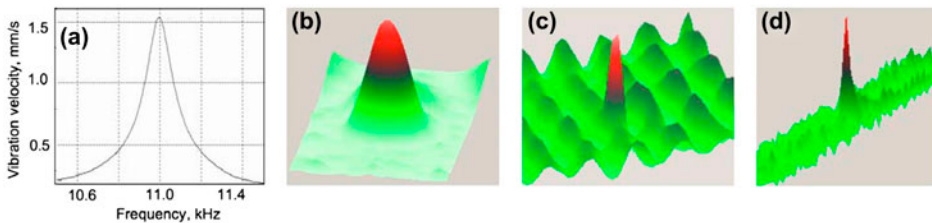


Figure 2. Frequency response (a) and vibration pattern for FBH in a PMMA specimen (b), 91160 Hz LDR of a delamination (c), and 110 kHz LDR for an impact damage (d) in CFRP specimens.

process is described by introducing the internal friction stress proportional to the velocity of strain variation that leads to a complex material elasticity  $E = E_1 + jE_2$  with imaginary part responsible for material dissipation. For low loss materials  $E_2$ , the dissipation module  $E_2 \approx \eta E$ , where  $\eta$  is the material loss factor. The complex material stiffness brings about a hysteretic stress-strain dependence (hysteretic damping model) with an area of the ellipse  $\Delta W = \pi \varepsilon_0^2 E_2$  equal to the energy damping in a unit volume of the material per a cycle of vibration. The number of cycles per second is  $\omega/2\pi$ , so that the heat energy generated per unit time (heat power) is:

$$P_H = \frac{\Delta W}{\Delta t} = \frac{\omega \varepsilon_0^2 \eta E}{2}. \quad (3)$$

According to (3), the heat power generated is proportional to the frequency ( $\omega$ ) and the square of the strain amplitude ( $\varepsilon_0$ ) of vibration. Therefore, the use of LDR, which strongly intensifies local vibrations, is beneficial for enhancing the efficiency of ultrasonic thermography.

It is instructive to note, that the polarization of the vibration is not worked out in the hysteretic damping approach. Note thereto that the high amplitude vibrations developed by LDR are polarized predominantly out-of-plane and therefore are readily detected by laser vibrometry as shown in Figure 2. The heat generation mechanism is concerned with internal friction, which is expected to be related to the in-plane vibration components. The evidence that the out-of-plane component of vibration is not directly involved in local heat generation is seen by comparing the LDR pattern for a FBH and the temperature induced pattern in the same defect (Figure 3). A smooth ‘bell-like’ LDR vibration profile inside the circular FBH (Figure 2(b)) generates a strong local heating in the centre surrounded by a temperature rise ring along the circumference (Figure 3).

The out-of-plane displacement ( $U(r)$ ) is nonetheless accompanied by the in-plane extension-compression deformation ( $\varepsilon_r$ ): it is zero in the middle plane of the plate and reaches maximal values on its both surfaces [4]:

$$\varepsilon_r = (d/2)(\partial^2 U(r)/\partial r^2), \quad (4)$$

where  $d$  is the thickness of the plate.

For a fundamental resonance, the radial distribution of  $U(r)$  in a circular FBH (radius  $R$ ) is given in [5]:

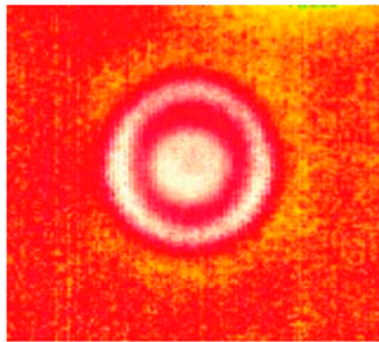


Figure 3. Temperature pattern generated by LDR vibrations in a circular FBH.

$$U(r) = \sum_{n=2} a_n (1 - (r/R)^2)^n. \quad (5)$$

Figure 4 shows that a close agreement between the calculations from (5) and the normalized LDR profile measurements are obtained by keeping only two terms in (5) and  $a_3 = 2a_2$ .

By substituting (5) in (4) the normalized radial distribution of the in-plane strain is calculated. Under assumption of the internal friction and the hysteretic damping approach (Equation (3)), the temperature profile and a local temperature rise generated by LDR vibrations can then be found by squaring the in-plane strain distribution. To this end, for a given vibration amplitude  $U(0)$  (measured by laser vibrometry) the absolute values of  $a_2$  and  $a_3$  are found from (5) and then used in calculating  $\varepsilon_r$  in (4). The values obtained are substituted in (3) to determine the heat energy generated in the defect and thus the temperature rise  $\Delta T$  in the defect over a certain insonation time  $t$ :

$$\Delta T = \frac{\omega \varepsilon_r^2 \eta E t}{2 \rho c_H}, \quad (6)$$

where  $E$  is Young's modulus,  $\rho$  is the mass density and  $c_H$  is the specific heat of the material.

The calculations of the temperature profile inside a circular FBH (LDR frequency 12480 Hz) in PMMA carried out from (4) to (6) for the following experimental parameters:  $R = 1$  cm;  $d = 1$  mm;  $t = 10$  s;  $U(0) = 8 \times 10^{-7}$ ;  $E = 4.8$  GPa;  $\eta = 0.02$  are shown in Figure 5 and compared with the experimental data (see Figure 3). A very close fit between the calculations and the results of measurements confirm a validity of the approach developed.

## 5. Efficiency of acousto-thermal conversion and feasibility of mW-LDR-thermosonics

According to Equation (6), to enhance efficiency of vibrothermography one should increase the local in-plane strain  $\varepsilon_r$  in the defect area. A traditional way to tackle the

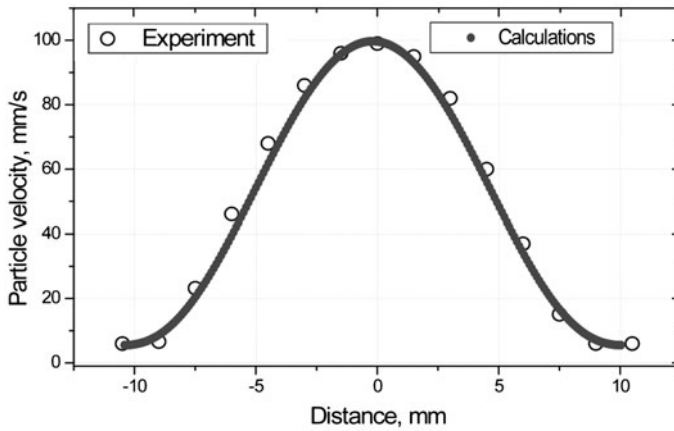


Figure 4. Profiles of LDR vibration pattern measured by laser vibrometry and calculated from Equation (5).

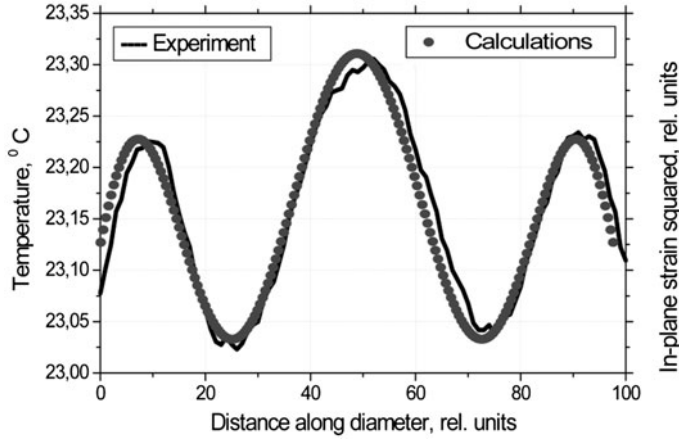


Figure 5. Temperature patterns generated by LDR vibrations in a circular FBH: measured and calculated from Equation (6).

problem, is to increase the input acoustic power used for excitation of the defect vibrations. Instead, in the LDR based thermosonics a local increase in  $\varepsilon_r$  is due to resonant ‘amplification’ of local defect vibrations achievable for a comparatively low input acoustic power  $P_{ac}$ . To quantify the benefit of LDR and to estimate realistic values of  $P_{ac}$  for a measurable temperature response, we introduce the LDR amplitude enhancement factor  $K = U_{LDR}/U_{IN}$  as the ratio of out-of-plane vibration amplitudes inside and outside LDR.

It is physically clear that in a general case, the increase in  $U_{LDR}$  (or  $K$ ) results in extra-bending and stronger extension-compression inside the LDR area and therefore cause an increase of the in-plane strain. This conclusion is readily seen for a FBH by combining (4) and (5) for a circular FBH to yield:

$$\varepsilon_r = 8U_{LDR}d/3R^2. \quad (7)$$

The excitation source is now introduced via its input acoustic power:

$$P_{ac} = \rho\omega^2 U_{IN}^2 cS/2, \quad (8)$$

where  $c$  is the acoustic wave velocity and  $S$  is the cross section area of the plate-like specimen.

By combining (7) and (8) the in-plane strain as a function  $P_{ac}$  is found and after substituting in (6) the temperature variation induced by LDR vibrations is obtained:

$$\Delta T = \frac{64K^2 d^2 \eta E t}{9\rho^2 c_H c S \omega R^4} P_{ac}. \quad (9)$$

Note, that for deriving (9) the expression for plane wave acoustic power (8) was used. Equation (9) is therefore directly applicable to elongated plate-like specimens with the wave propagation in a single direction; for omni-directional propagation (large specimens) cylindrical wave intensity ( $P_{ac}/S$ ) should be used.

In experiments, the effect of LDR on thermal response of defects was studied for a set of circular FBH of different sizes and LDR frequencies in PMMA plates. Unlike traditional thermosonic experiments, we used conventional disk-like piezoceramic transducers



attached (glued) to the specimen surface. The input voltage up to 90 V amplitude from HP 33120A function generator via a voltage amplifier HVA 3/450 was applied to the transducers to excite flexural waves in the frequency band up to 150 kHz. The wave amplitudes and velocities were monitored with a scanning laser vibrometer (vibration velocity mode) to evaluate a total acoustic power injected in the specimens. The thermal response of the defects was visualized and measured with an IR-camera (IRCAM Equus 327 K, NETD  $\approx$  15–20 mK).

Figure 6 shows the dynamics of the FBH LDR-thermal response: an accurate linear dependence on the input acoustic power agrees fully with theoretical expectations of Equation (3). The data also reveal an extremely high efficiency of the vibrothermal conversion: at  $\sim$ 200 mW input and 15 s-ultrasonic exposure, the temperature rise in the central part of the FBH amounts to  $\approx$ 3 K. To quantify the LDR-enhanced acousto-thermal conversion efficiency introduced as  $N = P_Q / P_{ac}$ , the power required for such heating is calculated as  $P_Q \approx 5 \times 10^{-3}$  W and for radiated acoustic power  $P_{ac} \approx$  200 mW their ratio yields:  $N \approx 2.5\%$ .

A crucial contribution of the LDR to the heating effect is clarified by measurements of the temperature rise in the defect area as a function of driving frequency (Figure 6). Even a slight (2–3%) detuning from an exact LDR frequency brings the temperature down to a basically non-measurable level of 10–20 mK and reduces the conversion efficiency by two orders of magnitude down to  $(1-2) \times 10^{-4}$ . Such a high-Q thermal response is a consequence of the quadratic nonlinearity involved in the acousto-thermal conversion (Equation (3)). This fact is illustrated in Figure 6 by a close fit between the acoustic LDR frequency response of the FBH (shown in Figure 2(a)) squared and its measured thermal response.

The results of similar measurements obtained for other FBH in PMMA specimens are summarised in Table 1. The data reveal that for low-mW input acoustic power (ranged from 1.6 to 63 mW) the temperature rise in the defects is substantially beyond the noise level ( $\Delta T$  between 50 and 460 mK) and is thus readily measurable. From (9), to compare and quantify the LDR contributions into thermal responses, the thermosonic quality factor of LDR is introduced as  $Q = K^2 / \omega c$  and given in Table 1. For FBH of similar configurations, the  $Q$  factor is proportional to their thermal responses for unit input  $P_{ac}$ . The  $Q$  values are also used in Table 1 for estimation of  $\Delta T$  from (9) for  $P_{ac}$

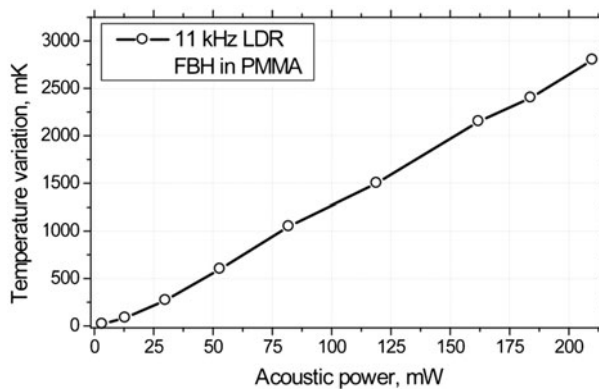


Figure 6. Temperature response of FBH as a function of input acoustic power at LDR frequency 11 kHz.

Table 1. LDR thermosonics for FBH in 4 PMMA specimens: experimental vs. calculated results.

N	$K^2$	$K^2/\omega c$ ( $10^{-6}$ ) ( $s^2 m^{-1}$ )	$P_{ac}$ measured (mW)	$\Delta T$ measured (K)	$\Delta T$ calculated (K)	$(P_{ac})_{min}$ calculated (mW)
1	45.3	1.3	63	$0.46 \pm 0.02$	0.26–0.52	3.9
2	377	9.9	4.6	$0.14 \pm 0.02$	0.15–0.3	1
3	437	23.8	1.6	$0.1 \pm 0.02$	0.13–0.26	0.5
4	57.3	1.2	8.5	$0.05 \pm 0.02$	0.03–0.064	5.1

used in the experiments. For PMMA Young’s modulus value  $E = 4.8$  GPa (obtained by measuring longitudinal and shear wave velocities in the specimens) and typical variation of  $\eta = (0.02\text{--}0.04)$  for PMMA,[6] a reasonable fit between the calculations (within the range of  $\eta$  variation) and the experimental  $\Delta T$  data is observed.

According to Table 1, the most efficient LDR thermosonics is observed for specimen PMMA3 (FBH with the highest  $K^2 = 437$ ) which exhibits a temperature rise of 0.1 K for only 1.6 mW of acoustic input. It is confirmed by the additional temperature measurement, which resulted in  $\Delta T = 0.44$  K for  $P_{ac} = 6.4$  mW, i.e. the LDR in this specimen is much more efficient heat producer than that in specimen 1. By introducing  $\Delta T$  30 mK as the lowest measurable thermal response, the minimum input  $P_{ac}$  can be evaluated from (9). The data in Table 1 confirm the feasibility of sub-mW LDR thermosonics for high  $Q$  defects (specimen 3) (Figure 7).

6. LDR thermosonic imaging

In this section, the enhancement of a defect thermal response by using the concept of LDR demonstrated above is applied to thermosonic imaging of defects. Conventional ultrasonic piezo-ceramic transducers (Conrad Elektronik GmbH) were used for excitation of defects in the strip-like specimens of 10–20 cm length producing a quasi-plane wave field. In larger specimens, the defects were activated by using mobile vacuum attached transducers (SI Scientific Instr. GmbH) which generated cylindrical flexural

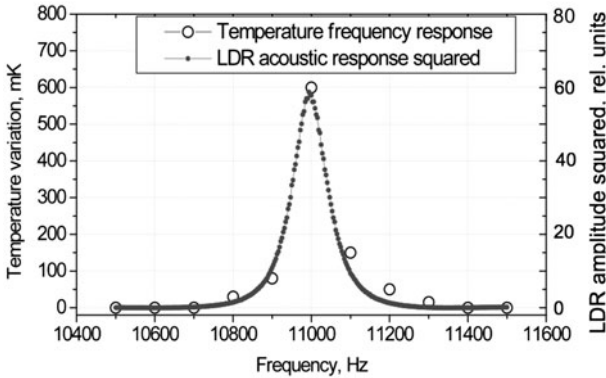


Figure 7. Temperature and acoustic response squared for FBH as a function of driving frequency.

waves. In all experiments, the acoustic power produced was monitored with a laser vibrometer and kept within mW-range.

Figures 8 and 9 show the results of LDR thermosonic imaging of a rectangular ( $2\text{ cm} \times 2\text{ cm}$ ) insert at 1.2 mm depth in ( $300\text{ mm} \times 300\text{ mm} \times 5\text{ mm}$ ) CFRP specimen. Figure 8 demonstrates a crucial role of LDR: At fundamental LDR frequency (8980 Hz) for 15 s insonation and 80 V input, the temperature response ( $\sim 0.25\text{ K}$ ) is by more than an order of magnitude higher than that outside the defect resonance (8000 Hz). The laser vibrometry measurements reveal both the fundamental (Figure 9(a); 8980 Hz) and the higher-order (Figure 9(b); 15600 Hz) LDR with substantially different vibration patterns. The thermal images taken at the corresponding excitation frequencies (Figure 9(c) and (d)) demonstrate the importance of the higher-order resonances for visualization of the shape of the defect: while the fundamental LDR visualizes the center part, the higher-order LDR are responsible for imaging of the border areas of the defect.

Figure 10 illustrates the application of the LDR thermosonics to an aluminum aviation component: ( $1.8\text{ mm} \times 180\text{ mm} \times 300\text{ mm}$ ) plate with a fatigue crack between the rivet holes (zoomed optical image Figure 10(a)). The identification of LDR of cracks in metals is complicated due to high mechanical quality factors of the materials and various vibration modes of the cracked defects. One of the LDRs of the fatigue crack measured by laser vibrometry at 11600 Hz is shown in Figure 10(b); the thermosonic image obtained at this frequency (Figure 10(c)) demonstrates the applicability of the LDR methodology to imaging of this kind of defects.

Another example of LDR thermosonics in composites is given in Figure 11 for a point-like impact damage (see Figure 2(d)) in a CFRP plate ( $270\text{ mm} \times 40\text{ mm} \times 1\text{ mm}$ ). The acoustic frequency response of the defect (Figure 11(a)) reveals fundamental LDR around 110 kHz. Unlike a smooth LDR frequency response for a ‘solid’ defect like FBH (Figure 2(a)), the resonance curve for impact damage displays ripples associated with resonances of weakly coupled parts of the defect. This effect is also evident in the thermal frequency response (Figure 11(b)).

The temperature rise measured in Figure 12(a) confirms highly efficient LDR thermosonics of impact damage in CFRP:  $\Delta T = 1.4\text{ K}$  for  $\sim 60\text{ mW}$  input acoustic power. Such a temperature variation provides an opportunity for reliable LDR thermosonic

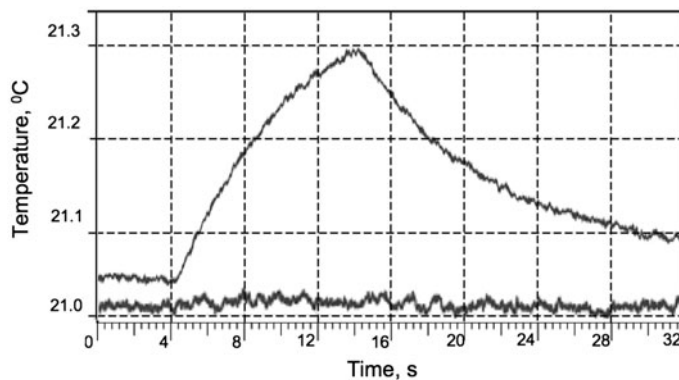


Figure 8. Temperature response of a rectangular insert in CFRP plate at LDR frequency (8980 Hz, upper curve) and outside resonance (lower curve, 8000 Hz).

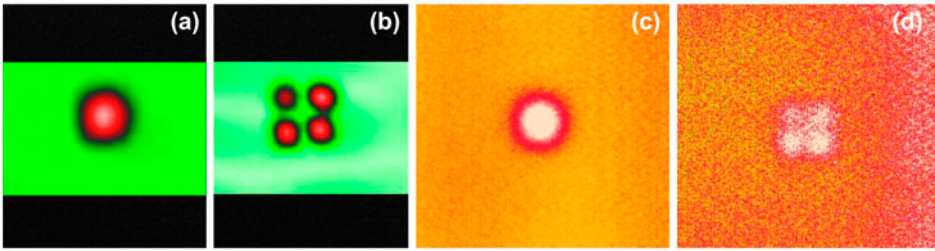


Figure 9. Laser vibrometry (a, b) and thermosonic (c, d) images of a rectangular insert in CFRP plate at fundamental LDR frequency (8980 Hz, (a, c)) and at higher-order LDR (15600 Hz, (b, d)).

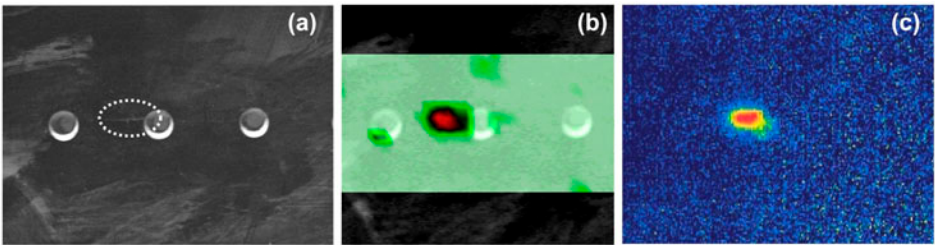


Figure 10. Laser vibrometry (b) and LDR thermography (c) imaging of fatigue crack between the rivet holes (dotted area in zoomed optical image (a)) in aluminum aviation component.

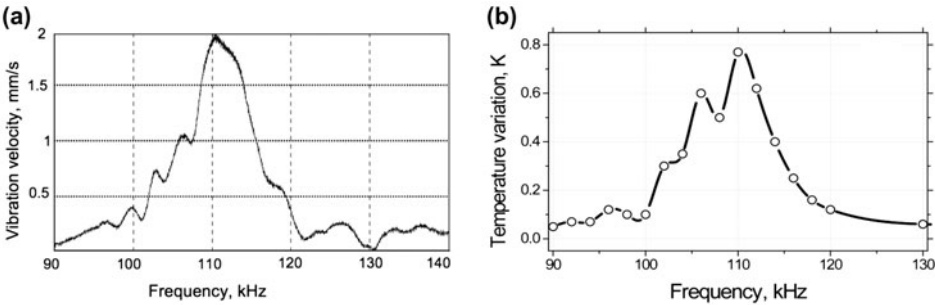


Figure 11. Acoustic (a) and thermal (b) LDR frequency responses of an impact induced damage in CFRP plate.

imaging in mW power range (Figure 12(b)) with a high temperature contrast in lateral direction (Figure 12(a)).

The results shown above imply that a strong increase in the defect temperature rise (thermal output signal) at LDR frequency enhances the signal-to-noise ratio (SNR) of thermosonic imaging. On the other hand, an increase of the SNR is also known to occur in the lock-in mode primarily due to diminishing the noise level.[7] By introducing the benefit of LDR in the lock-in approach a resonance thermosonic mode operating at unusually low excitation levels can be projected. To this end, following the general lock-in concept the amplitude of ultrasonic excitation at the LDR frequency

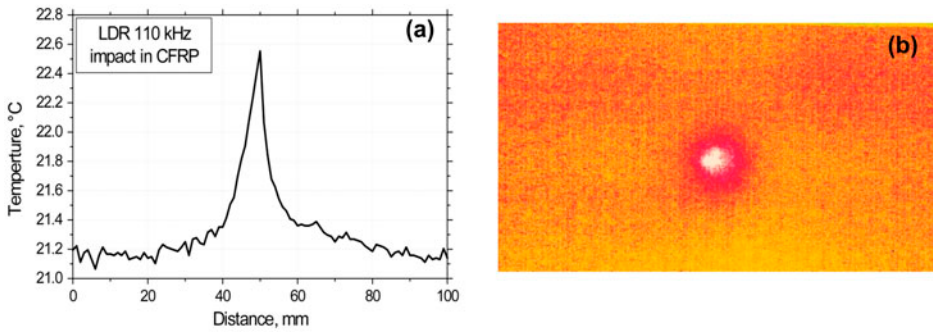


Figure 12. LDR thermosonic imaging of  $\sim(5 \text{ mm} \times 5 \text{ mm})$  impact damage area in a CFRP plate (b); quantified temperature contrast of the image (a).

was modulated sinusoidally by the lock-in frequency (between 0.01 and 1 Hz). A temperature image sequence of the surface was recorded with the IR-camera and a discrete Fourier transformation at the lock-in-frequency was applied to compress this image sequence into a pair of amplitude and phase images.

An enhancement in sensitivity and the SNR of the LDR lock-in imaging are readily seen from Figure 13, where the amplitude lock-in (a) and LDR temperature (b) thermosonic images of the FBH (specimen N3, Table 1) are shown. To have the SNR  $>1$  in the temperature image (Figure 13(b)), the input power had to be increased up to  $\sim 2 \text{ mW}$  (to generate  $\Delta T \sim 100 \text{ mK}$ ). On the contrary, the LDR lock-in image in Figure 13(a) was taken when the input was reduced to anomalously low power of  $\sim 200 \text{ mW}$ . The background for such an extraordinary performance is a combined action of the lock-in (reduction of noise) and the high thermosonic quality factor (efficient heat generation) in the LDR for this FBH (see Table 1).

In Figure 14(a) and (b), the enhancement in sensitivity of thermosonics by combining LDR and lock-in is illustrated for an impact damage in a CFRP plate: the amplitude lock-in image (a) corresponds to  $\sim 1 \text{ mW}$  input power while a similar contrast of the temperature image (b) requires  $\sim 16 \text{ mW}$  of acoustic power.

## 7. LDR non-contact thermosonics

Such an efficient ultrasonic activation of defects enables to proceed with a remote thermosonic mode by using air-coupled ultrasonic (ACU) excitation. For this purpose, we used the Ultrac ACU transducers whose fundamental frequencies ( $\sim 50$  and  $\sim 70 \text{ kHz}$ )

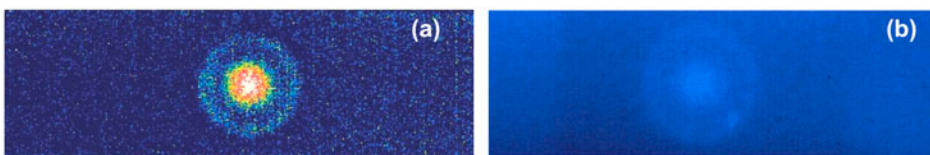


Figure 13. LDR thermosonic imaging of FBH in PMMA plate at LDR frequency 7670 Hz: (a) amplitude lock-in (lock-in frequency 0.05 Hz) image (acoustic input  $\sim 200 \text{ mW}$ ); (b) temperature image at input power  $\sim 2 \text{ mW}$ .



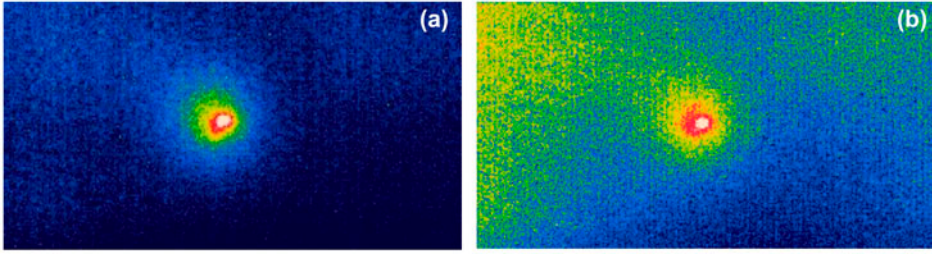


Figure 14. LDR thermosonic imaging of an impact ( $\sim 5 \text{ mm} \times 5 \text{ mm}$ ) in CFRP plate: amplitude lock-in image (a) at  $\sim 1 \text{ mW}$  input acoustic power; (b) temperature image at  $\sim 16 \text{ mW}$  input power.

match the LDR frequencies of defects. The transducers were placed a few cm away from the defect area, while the IR-image was observed from the opposite side of the plate specimen (ACU-IR non-contact ‘through- transmission’ mode) (Figure 15(a)). The AC-radiometer methodology [8] was employed to measure the ACU power ( $P_{\text{ACU}}$ ) radiated.

The temperature response of a FBH in PMMA plate measured for input ACU power of  $\sim 50 \text{ mW}$  and 30 s insonation pulse is shown in Figure 15(b): the temperature rise in the FBH area amounts to  $\sim 0.6 \text{ K}$  that is far beyond the sensitivities of modern IR-cameras. The dynamics of ACU thermosonics is shown in Figure 16(a) and demonstrates that reliable defect detection is feasible for even lower ACU power (down to few mW).

The ACU thermosonic image of this FBH (3 mm radius, 1 mm thickness, 50.2 kHz LDR) in a PMMA plate ( $170 \text{ mm} \times 50 \text{ mm} \times 10 \text{ mm}$ ) is shown in Figure 16(b). The data in Figure 16(a) were used to calculate the power ( $P_Q$ ) required for heating the defect and to evaluate the efficiency of ACU thermosonics mode (averaged on the measurement points):  $N_{\text{ACU}} = P_Q/P_{\text{ACU}} \approx 0.8\%$ .

An example of ACU imaging of realistic defects is illustrated in Figure 17 for an impact damage (LDR frequency  $\sim 69.6 \text{ kHz}$ ) in 1.1 mm-thick multi-ply CFRP plate. To improve the sensitivity of thermosonics, the LDR excitation was combined with lock-in image processing. The ACU thermosonic phase images of the circular shape damage (radius  $\sim 12 \text{ mm}$ ) induced on the rear side of the impact are shown in Figure 17 and taken in the lock-in mode for the input ACU power of  $\sim 7 \text{ mW}$ . The laser vibrometry

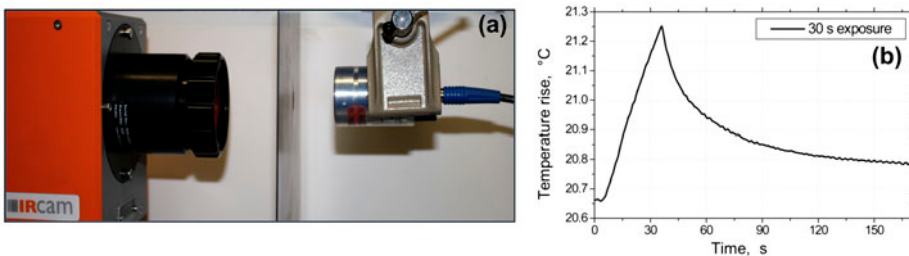


Figure 15. ‘Through-transmission’ non-contact ACU thermosonics set-up (a), temperature response of FBH to 50 mW ACU excitation at LDR frequency 50.2 kHz (b).

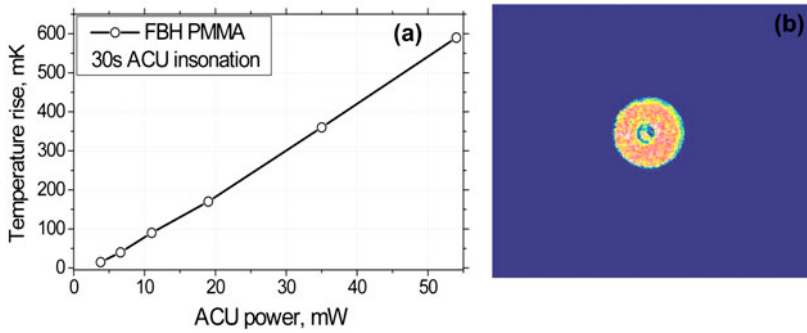


Figure 16. Temperature response of a circular FBH to ACU excitation (a), ACU LDR thermosonic image of a circular FBH in PMMA plate (b).

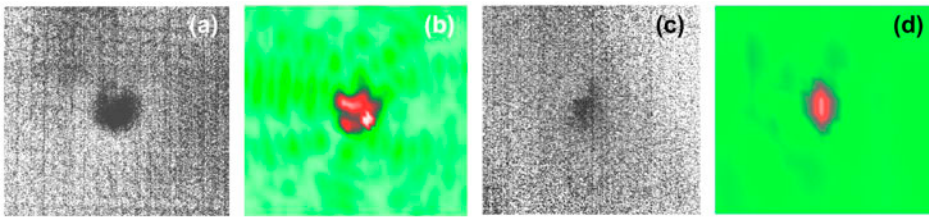


Figure 17. Noncontact ACU LDR thermosonic (a, c) and laser vibrometry (b, d) imaging of an impact area (~12 mm diameter) in CFRP plate at different frequencies: (a, b) ACU excitation at LDR frequency of 69.6 kHz; (c, d) ACU frequency 69 kHz.

images are given in Figure 17 for comparison. When the input ACU frequency matches exactly the LDR frequency (69.6 kHz), both the techniques reveal the total circular impact area reliably (Figure 17(a) and (b)). A minor mismatch between the excitation and the LDR frequencies (0.6 kHz) results in the contraction of both images with only the core part of the impact visible. The similarity in the frequency behaviour of the laser vibrometry and ACU LDR images confirms the practical relevance of non-contact ACU thermosonics.

## 8. Conclusions

In ultrasonic thermography, the defect thermal response is caused by a local dissipation of mechanical energy, which is converted into heat. For viscoelastic materials, this process is described by the hysteretic damping model, which shows that the heat power generated is proportional to the frequency and the square of the strain amplitude of vibration. Therefore, the use of LDR, which strongly intensifies local vibrations, is beneficial for enhancing the efficiency of vibro-thermography. A traditional way to tackle the problem, is to increase the input acoustic power used for excitation of the defect vibrations. Instead, in the LDR based thermosonics, a local increase in the strain is due to resonant ‘amplification’ of local defect vibrations ( $K$ ) achievable for a comparatively low input acoustic power. The LDR contribution to the defect thermal response is proportional to  $K^2$  and can enhance the acousto-thermal conversion by one to two orders of magnitude.

The case studies of LDR thermosonics for simulated (FBH) and realistic defects (delaminations, impacts, cracks) in metals and composites confirm the feasibility of high contrast imaging in the mW-power range. Further enhancement of sensitivity and SNR of thermosonic images is achieved by using LDR in the lock-in image processing mode. This enables to proceed to remote thermosonic imaging by using an ACU excitation of defects.

In summary, the application of LDR concept enhances substantially the efficiency of vibro-thermal conversion in ultrasonic thermography. The LDR thermosonics requires much lower acoustic power to activate defects that makes it possible to avoid high-power ultrasonic instrumentation and proceed to a non-contact imaging mode by using ACU excitation.

### Acknowledgements

One of the authors (Igor Solodov) acknowledges support of this study in the framework of ALAMSA project funded from the European Union's Seventh Framework Programme for research, technological development and demonstration under grant agreement no. 314768.

### Disclosure statement

No potential conflict of interest was reported by the authors.

### References

- [1] Mignogna RB, Green RE Jr, Duke JC, Henneke EG II, Reifsnider KL. Thermographic investigation of high-power ultrasonic heating in materials. *Ultrasonics*. 1981;19:159–163.
- [2] Solodov I, Bai J, Bekgulyan S, Busse G. A local defect resonance to enhance acoustic wave-defect interaction in ultrasonic nondestructive evaluation. *Appl. Phys. Lett.* 2011;99:211911.
- [3] Solodov I, Bai J, Busse G. Resonant ultrasound spectroscopy of defects: Case study of flat-bottomed holes. *J. Appl. Phys.* 2013;113:223512.
- [4] Landau LD, Lifshitz EM. *Theory of elasticity*. Pergamon Press; 1959.
- [5] Timoshenko SP. *Vibration problems in engineering*. 4th ed. New York (NY): D. Van Nostrand Company; 1956.
- [6] Lakes R. *Viscoelastic materials*. New York (NY): Cambridge University Press; 2009.
- [7] Rantala J, Wu D, Busse G. Amplitude-modulated lock-in vibrothermography for NDE of polymers and composites. *Res. Nondestr. Eval.* 1996;7:215–228.
- [8] Solodov I, Döring D, Busse G. Air-coupled laser vibrometry: analysis and applications. *Appl. Opt.* 2009;48:C33–C37.